Pressure and Temperature Dependence of the Dilute Solution Segmental Dynamics of Anthracene-Labeled Polyisoprene

B. J. Punchard and D. B. Adolf*

Department of Physics and Astronomy, University of Leeds, Leeds, LS2 9JT United Kingdom

Received October 12, 2001; Revised Manuscript Received January 7, 2002

ABSTRACT: The local segmental dynamics of anthracene-labeled *cis*-1,4-polyisoprene in dilute solution have been studied as a function of temperature (298−323 K) and pressure (0.1−150 MPa) in several solvents (dioctyl phthalate, *n*-dodecane, squalane, and toluene). This range of temperature and pressure afforded a viscosity range of 0.55−494 mPa·s. Previous studies of *cis*-1,4-polyisoprene as a function of temperature at ambient pressure have revealed that these motions scale as a fractional power of the solvent viscosity, η, thereby violating Kramers' theory which predicts $\tau_c \sim \eta$. Findings reveal quantitatively similar behavior is observed when the solvent viscosity is varied by pressure at fixed temperatures.

I. Introduction

Efforts to understand the structure−property relationships of polymers have focused on local segmental dynamics. These polymer dynamics occur on the length scale of a few repeat units and are influenced by the chemical structure of the repeat unit. These short length scale motions have been experimentally monitored in the solution to bulk state by techniques such as dielectric relaxation,[1−11] NMR,[12−14] and time-resolved optical spectroscopy [TROS].[15−22] Within solutions, it is observed that the dynamics scale by a fractional power of solvent viscosity, η. For example, the local motions of *cis*-1,4-polyisoprene monitored as a function of temperature by TROS[19] scale as $\eta^{0.75\pm0.05}$ within a study using nine solvents spanning more than 2 decades in viscosity. ^{13}C NMR measurements[13] on *cis*-1,4-polyisoprene reveal local dynamics that scale as $\eta^{0.41\pm0.02}$. The two techniques yield different scaling behavior since they are sensitive to different sources of local motions. The TROS experiments probe the local dynamics associated within an electronic transition dipole oriented parallel to the polymer backbone, while NMR probes the local dynamics associated with C−H or C−D bond vectors oriented more transverse to the polymer backbone. The salient feature to note is that results from both studies violate Kramers' theory[23] which predicts that the dynamics would scale by $\eta^{1.00}$. For systems where the polymer and solvent motional time scales are well separated, this scaling of the local motions by the first power of solvent viscosity is observed, such as for the dilute solution local segmental dynamics of polystyrene.[24] Scaling of local dynamics by a fractional power of the solvent viscosity (i.e., *cis*-1,4-polyisoprene, $\eta^{0.41\pm0.02}$) is observed when this time scale separation is not fulfilled.

To date, studies of the solvent viscosity scaling of dilute solution local polymer dynamics have employed a variety of solvents and have been performed as a function of temperature only. Surprisingly, the role of pressure has not been addressed. High-pressure investigations of small molecule isomerization within *n*-alkane solvents (i.e., 2-vinylanthracene[25] (2VA) and 2-(2-propenyl)anthracene[26] (22PA)) using TROS have revealed kinetics which also violate Kramers' theory. Findings also revealed that the activation volumes for the isomerization of 2VA,[25] the isomerization of 3,3′-diethyloxadicarbocyanine iodide,[27] and the intramolecular excimer formation of 1,3-di(1-pyrenyl)propane[28] were negligible with the observed pressure dependence of the isomerization dynamics being dominated by the activation volume attributed to the solvent. The current work describes an analogous study employing TROS to investigate the viscosity scaling of the local dynamics of anthracene labeled *cis*-1,4-polyisoprene in dilute solution as a function of both temperature and pressure, utilizing four different solvents over a temperature range of 298−323 K and a pressure range of 0.1−150 MPa. Section II discusses the experimental technique in greater detail with results and discussion presented in section III. A summary is found in section IV.

II. Method

Materials and Sample Preparation. Anthracene center labeled *cis*-1,4-polyisoprene (PI*) used in this study was synthesized at Durham University (Prof. R. Richards, Ms. A. Keeny, and Mr. T. Keef). Each polymer chain contains one chromophore covalently bonded in the middle of the chain (see Figure 1). The $S_0 \rightarrow S_1$ electronic transition dipole moment of the chromophore is oriented along the chain backbone. Any movement of the dipole reflects movement of the polymer backbone. The polyisoprene used has M_w = 108 000 and a polydispersity of 1.20 obtained via size exclusion chromatography and static light scattering. The chain microstructure determined by NMR was found to be 71% cis 1,4 units, 23% trans 1,4 units, and 6% vinyl 1,2 units.

Solutions of PI* were prepared at concentrations of ≤0.5 wt % to give an optical density of ∼0.1 in a 3 mm path length cuvette at 406 nm. To avoid fluorescence quenching, the solution was subjected to three freeze−pump−thaw cycles to replace molecular oxygen with molecular nitrogen. The solvents employed were toluene, *n*-dodecane, squalane, and dioctyl phthalate, and all were used as received (Aldrich; all >99% purity). The viscosities of the solvents at ambient pressure (i.e., 0.1 MPa) are taken from the literature.[13,29,30] High-pressure viscosity data for these solvents were supplied by Dr. N. F. Glen of the National Engineering Laboratory.[31] Equations describing the pressure dependence at different temperatures of the solvents used in this study are found in Table 1. These data were generated using torsionally vibrating crystal viscometry,[32] falling body viscometry,[33] and rolling ball viscometry[34] and have an associated error of ±2%.

High-Pressure Cell. The high-pressure cell used in this study was purchased from ISS Inc., Champaign, IL. The cell consists of a drilled stainless steel alloy block with four window ports and a top plug for removal and replacement of samples.

* To whom correspondence should be addressed. Telephone 0113 2333812; Fax 0113 2333846; e-mail D.B.Adolf@leeds.ac.uk.

10.1021/ma011783r CCC: $22.00
Published on Web 03/13/2002

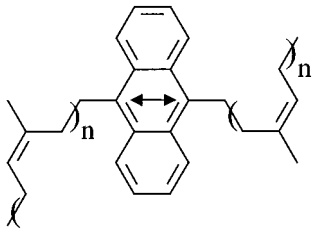

Figure 1. Structure of anthracene-labeled polyisoprene. The $S_0 \rightarrow S_1$ transition is indicated by the double-headed arrow.

Table 1. Fit Parameters for the Isotherm of the Viscosity Data for Each Solvent Given in the Form $\ln(\eta/\eta_0) = \sum_{i=1}^{n} \nu_i(P - P_0)^i$, Where η_0 Is the Viscosity of the Solvent at a Pressure of $P_0 = 0.1$ MPa[a]

solvent	temp [K]	$10_3 \times \nu_1$	$10^6 \times \nu_2$	$10^9 \times \nu_3$	η_0 [mPa·s]
toluene	298	7.412	−8.571	8.916	0.552
	313	6.826	−3.407		0.474
	323	7.675	−11.579	11.851	0.421
n-dodecane	298	12.316	−19.789		1.354
	313	11.470	−17.855	11.202	1.070
	323	11.031	−18.340	24.763	0.928
squalane	298	22.248	−23.869	9.503	29.120
	313	20.430	−21.700	8.378	16.200
	323	20.340	−20.929	6.447	11.500
dioctyl phthalate	298	22.403	−20.505	18.963	58.600
	313	20.537	−18.056	14.609	29.210
	323	18.850	−15.801	11.152	16.900

[a] The data are fitted with a standard deviation of less than 2%.

The 10 mm clear aperture quartz windows are 8.5 mm thick and used as supplied with the cell. With these windows, the cell can be pressurized up to 300 MPa with a maximum working temperature of 333 K. This paper reports data taken at temperatures of 298, 313, and 323 K and at pressures of 0.1, 40, 100, and 150 MPa at each of the three temperatures. Channels through the cell connected to an external bath allow temperature control to ±1 K. The pressurizing medium is spectroscopic grade ethanol with the hydrostatic pressure generated by a hand pump.

Experimental Technique. The experimental technique[35] and apparatus[20] are described in detail elsewhere, and only a brief description is given here. A short polarized pulse of light is used to photoselect an anisotropic distribution of the anthracene chromophores. Chromophores with their $S_0 \rightarrow S_1$ electronic transition dipole moments parallel to the excitation polarization are preferentially excited. Since the excited-state chromophores emit light directed along the transition dipole moment, fluorescence emission immediately after excitation is polarized. Within this study, the excitation wavelength is 406 nm and the emission wavelength is 414 nm. Local segmental polymer dynamics are observed by monitoring the time-resolved decay of the polarization of the emission fluorescence both parallel, $I_{\parallel}(t)$, and perpendicular, $I_{\perp}(t)$, to the polarization of the excitation pulse using time-correlated single photon counting techniques.

A time-dependent anisotropy function, $r(t)$, is calculated from these emission decays as

$$r(t) = \frac{I_{\parallel}(t) - I_{\perp}(t)}{I_{\parallel}(t) + 2I_{\perp}(t)} \tag{1}$$

The measured anisotropy is directly related to a second-order orientational autocorrelation function, $CF(t)$, as

$$r(t) = r_0 CF(t) = r_0 \langle P_2(\cos\theta(t)) \rangle \tag{2}$$

where r_0 is the fundamental anisotropy, P_2 is the second Legendre polynomial, and $\theta(t)$ is the angle through which a transition dipole moment has rotated in time t since the excitation pulse.

Data Fitting. Distortions in the data introduced by the finite width of the laser pulse (~5 ps) and the response of the detection equipment were deconvolved from the data by iterative impulse reconvolution.[36] The anisotropy decays were then fit to an empirical biexponential function with fitting parameters A, B, τ_1, and τ_2.

$$r(t) = A \exp(-t/\tau_1) + B \exp(-t/\tau_2) \tag{3}$$

The biexponential fits are used only to characterize the shape of the anisotropy decays, and no further significance is given to the fit parameters.

Reduced χ^2 values for these fits were typically ≤1.1. The overall time scale of the monitored segmental dynamic is determined via a correlation time, τ_c, of the decay defined as

$$\tau_c = \frac{1}{r_0}\int_0^{\infty} r(t)\, dt \tag{4}$$

Values of τ_c are determined via integration of the biexponential fits. Errors in τ_c reported within this paper are ±10% based on repeated measurements. The value of r_0 for measurements at atmospheric pressure in this study was found to be 0.33 ± 0.02, in good agreement with values for other anthracene-labeled polymers found elsewhere.[19,24]

Correction of Pressure-Induced Birefringence. A correction to the experimental values of $I_{\parallel}(t)$ and $I_{\perp}(t)$ is required due to pressure-induced birefringence of the quartz windows. Polarization scrambling caused by the birefringence is accounted for by the well-known[37−43] method of Paladini and Weber.[44] This method utilizes a fluorophore which is immobile over the pressure range employed within the experiment. Employing eq 10 from ref 44, the following expression was derived for the true anisotropy, $r(t)$, in terms of the observed anisotropy, $r'(t)$, and a single scrambling factor, γ.

$$r(t) = r'(t)\left(\frac{1}{1 - 3\gamma}\right) \tag{5}$$

It was assumed that the pressure-induced birefringence in the excitation and emission windows is equal at each pressure.[44] Neglect of terms on the order of γ^2 within the resulting expression afforded corrected anisotropies that differed by no more than 2% when compared to anisotropies corrected with the inclusion of terms involving γ^2.

The scrambling correction factor, γ, is determined at a pressure P by comparing the emission anisotropy value of a rotationally immobile fluorophore at P, $\langle r \rangle_P$, with its emission anisotropy value at atmospheric pressure, $\langle r \rangle_{atm}$, via

$$\gamma = \frac{1}{3}\left[1 - \frac{\langle r \rangle_P}{\langle r \rangle_{atm}}\right] \tag{6}$$

The scrambling factors were determined using PI* in dioctyl phthalate at 283 K with results denoted as open circles in Figure 2. Also shown in Figure 2 are scrambling factors based on DPA (diphenylanthracene, inverted triangles) in methylcyclohexane at 298 K, DMA (dimethylanthracene, triangles) in methylcyclohexane at 298 K, and PI* (diamonds) in toluene at 298 K. Similar data reported by Paladini and Weber[44] for fluorescein (closed squares) in glycerol at 248 K are also shown for comparative purposes. Scrambling factors obtained from the DPA/methylcyclohexane, DMA/methylcyclohexane, and PI*/toluene systems used only values of the fundamental anisotropy, r_0, at atmospheric and higher pressures for the steady-state emission anisotropy values $\langle r \rangle_{atm}$ and $\langle r \rangle_P$ in eq 6, respectively. Good agreement is observed between these systems and the PI*/dioctyl phthalate system. The solid and dashed curves running through the data are third-degree polynomial fits to the current data (solid) and to the data of Paladini and Weber[44] (dashed). The general shapes of these two curves are observed to be qualitatively similar. Quantitative differences are due to equipment specific factors such as the window material and the window thickness. The value of

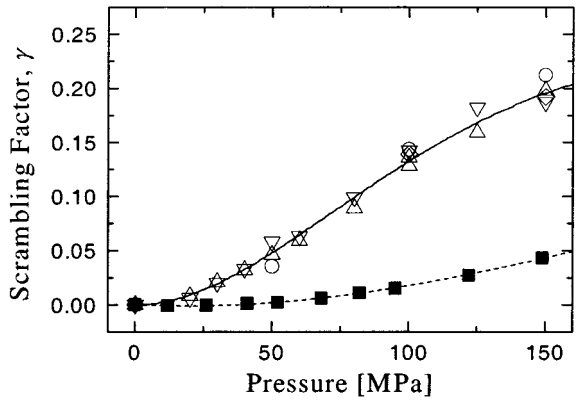

Figure 2. Scrambling factors as a function of pressure. Symbols refer to DPA (inverted triangles) and DMA (triangles) in methylcyclohexane at 298 K, PI* in toluene at 298 K (diamonds), and PI* in dioctyl phthalate at 283 K (circles). Also shown are the correction factors found by Paladini and Weber[44] (solid squares) for fluorescein in glycerol at 248 K. The solid and dashed lines are third-degree polynomial fits to the data.

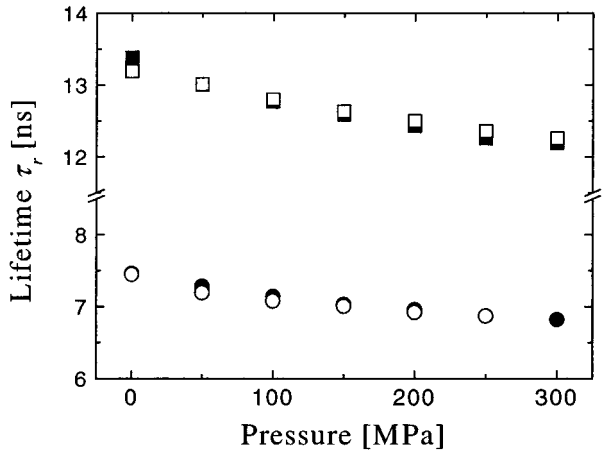

Figure 3. Natural radiative lifetimes of DMA (squares) and DPA (circles) under pressure. Open symbols are the current optical data, and the solid symbols refer to the work of Hirayama et al.[45]

r_0 for all data after correction was found to be 0.31 ± 0.02 averaged over all pressures and temperatures studied. The actual values of the scrambling factors employed to perform the birefringence correction of the data are generated from the solid best-fit curve in Figure 2.

Pressure Dependence of Anthracene Lifetimes. The pressure dependence of the fluorescence lifetime of anthracene was investigated at high pressure using DMA and DPA. Results from this study are plotted in Figure 3 as open symbols with similar results from Hirayama et al.[45] plotted as closed symbols. Excellent agreement between the two sets of data is observed. This agreement between these measurements at high pressure serves as a valuable indication that the solution samples within this study are experiencing the desired hydrostatic pressure.

Data Reproducibility. To obtain data at a temperature T_1 and a pressure P_1, the cell was first equilibrated at the desired temperature T_1 and atmospheric pressure for approximately 1 h. The pressure was then increased in approximately 20 MPa increments until P_1 was reached while holding the temperature at T_1. At each 20 MPa increase in pressure, the cell was allowed to stand for another 2−3 min before data were taken. The size and mass of the high pressure cell required reasonably lengthy temperature equilibration periods relative to the time required for pressure equilibration. This data acquisition protocol avoids lengthy temperature equilibration at a high pressure, thereby reducing wear and tear on the quartz windows. Correlation times for three separately prepared samples of *cis*-1,4-polyisoprene in toluene as a function of pressure at 298 K are illustrated in Figure 4. Reproducibility is observed to be excellent. Reproducibility is further confirmed when this protocol is performed on a same sample for a second time. This can be observed in Figure 4 when comparing open circles and open triangles relative to closed circles and closed triangles, respectively.

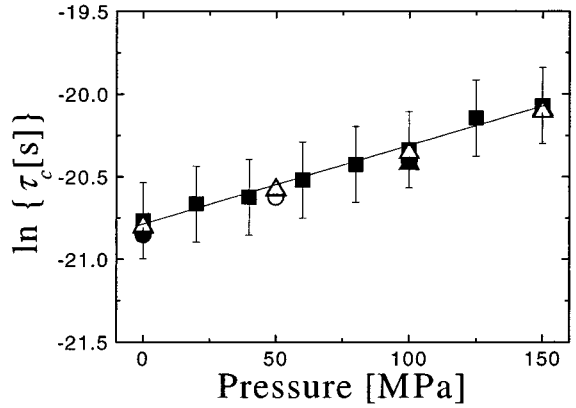

Figure 4. Correlation times as a function of pressure for anthracene-labeled *cis*-1,4-polyisoprene in toluene at 298 K. Data shown represent that taken on three separately prepared samples (squares, circles, and triangles). The open symbols are data taken on a second pressurization of that sample. The solid line is a best fit to all the data.

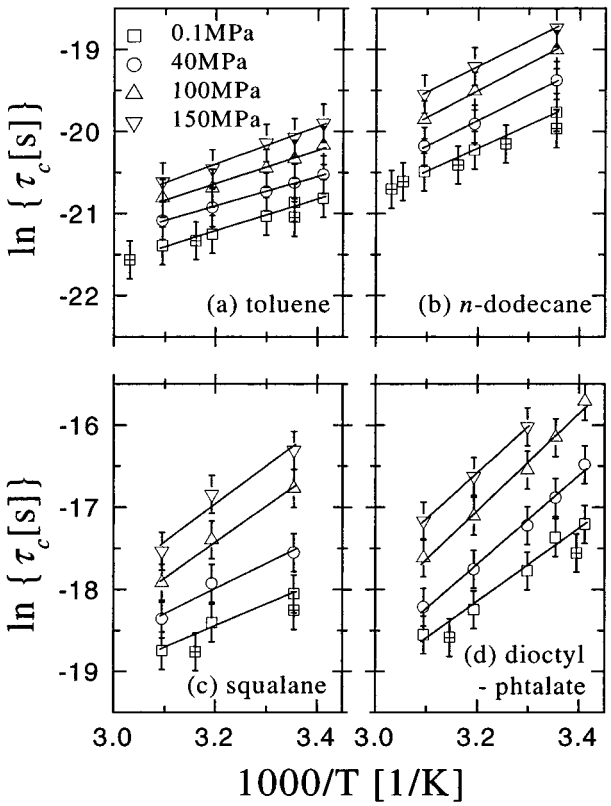

Figure 5. Correlation times for the dilute solution local segmental dynamics of anthracene-labeled *cis*-1,4-polyisoprene plotted in Arrhenius format. The solvents are (a) toluene, (b) *n*-dodecane, (c) squalane, and (d) dioctyl phthalate at 0.1 MPa (squares), 40 MPa (circles), 100 MPa (triangles), and 150 MPa (inverted triangles). Also shown as crossed squares on each plot are data for each solvent at 0.1 MPa from Adams.[46] The solid lines are best fits to the data, and the slope of each line is related to the experimental activation energy, E_{obs}, for *cis*-1,4-polyisoprene local dynamics at that pressure.

Table 2. Observed Arrhenius Activation Energies, E_{obs}, Determined from the Slopes of Figure 5 as a Function of Pressure[a]

press. [MPa]	E_{obs} [kJ mol^{-1}]			
	toluene	*n*-dodecane	squalane	dioctyl phthalate
0.1	12	23	22	37
40	15	26	25	45
100	17	27	36	49
150	19	26	38	47

[a] There is an error of ±10% associated with each value.

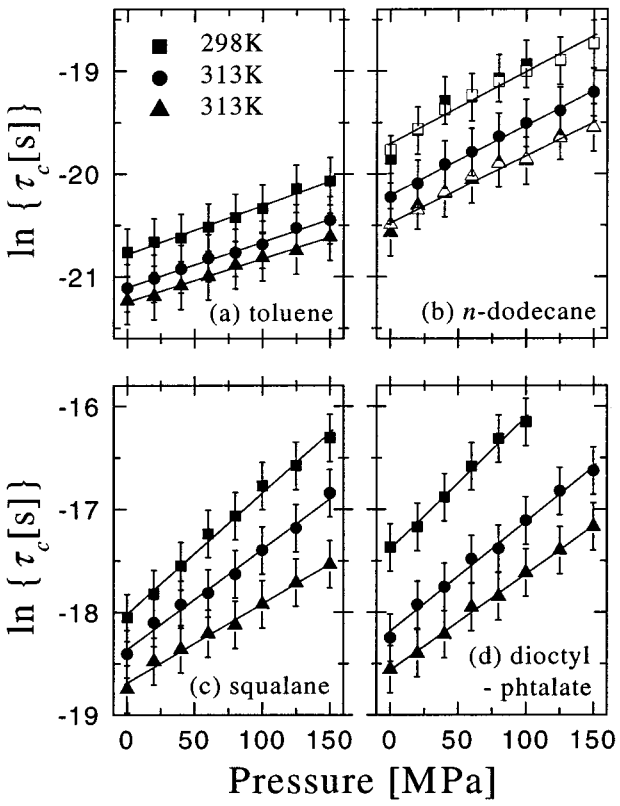

Figure 6. Correlation times for the dilute solution local segmental dynamics of anthracene-labeled *cis*-1,4-polyisoprene as a function of pressure. The solvents are (a) toluene, (b) *n*-dodecane, (c) squalane, and (d) dioctyl phthalate at 298 K (squares), 313 K (circles), and 323 K (triangles). Open symbols represent repeat data taken on a different sample at a different time. The solid lines are best fits to the data, and the slope of each line is related to the experimental activation volume, V_{obs}, for *cis*-1,4-polyisoprene local dynamics at that temperature. It is important to note that each best fit line describes the data well both at low pressures where the birefringence correction is minimal and at high pressure where this correction becomes more significant.

III. Results and Discussion

Figure 5 reveals plots of ln τ_c vs 1000/T at 0.1, 40, 100, and 150 MPa within toluene (Figure 5a), *n*-dodecane (Figure 5b), squalane (Figure 5c), and dioctyl phthalate (Figure 5d). Open symbols are data taken for this study where open symbols with interior crosses are from an earlier independent study at atmospheric pressure only.[46] Each best-fit line running through the data affords the observed activation energy, E_{obs}, for local polymer dynamics within the indicated solvent at the indicated pressure. Values of E_{obs} are found in Table 2. For a given solvent, the local dynamics are slowest at low temperatures and high pressures. Motions are observed to slow by a factor of 2 when temperature decreases over the range 298−323 K in toluene and by a factor of 4 in dioctyl phthalate. In the pressure regime, motions slow by a factor of 2 when increasing pressure over a range of 0.1−150 MPa in toluene and a factor of 3 in dioctyl phthalate over a range of 0.1−100 MPa. Figure 6 reveals plots of ln τ_c vs pressure at 298, 313, and 323 K within toluene (Figure 6a), *n*-dodecane (Figure 6b), squalane (Figure 6c), and dioctyl phthalate (Figure 6d). Closed symbols are data taken for this study whereas open symbols represent repeat measurements on a different sample. Each best-fit line running through the data affords the observed activation volume, V_{obs}, for local polymer dynamics within the indicated solvent at the indicated temperature. Values of V_{obs} are found in Table 3. It is important to note that data taken at low pressure with minimal birefingence correction are in good agreement with high-pressure data where the correction becomes larger.

Table 3. Observed Activation Volumes, V_{obs}, Determined from the Slopes of Figure 6 as a Function of Temperature[a]

temp [K]	V_{obs} [cm^3 mol^{-1}]			
	toluene	*n*-dodecane	squalane	dioctyl phthalate
298	12	16	29	32
313	12	17	26	28
323	11	16	24	25

[a] There is an error of ±10% associated with each value.

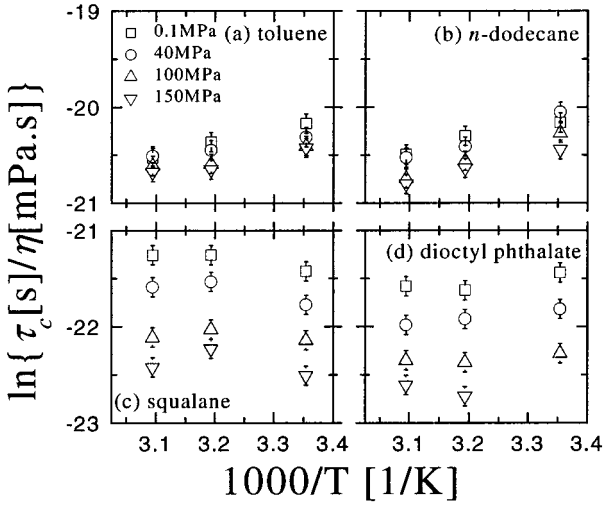

Figure 7. Plots of ln(τ_c/η) as a function of 1000/T illustrating the failure of Kramers' theory in the high friction limit. The solvents are (a) toluene, (b) *n*-dodecane, (c) squalane, and (d) dioctyl phthalate at 0.1 MPa (squares), 40 MPa (circles), 100 MPa (triangles), and 150 MPa (inverted triangles).

Kramers' theory[23] predicts activated solution state dynamics within the high friction limit scale linearly with solvent viscosity as follows

$$\tau_c \sim \eta \exp(E_a/RT) \qquad (7)$$

where E_a is the activation energy associated with the motion and R is the gas constant. Differences between E_{obs} and E_a are attributed to contributions from the solvent through its activation energy of viscous flow. The motions within this study are observed to violate Kramers' theory as illustrated in Figure 7 for dynamics as a function of temperature. Rather than a straight line whose slope would be related to E_a, the temperature dependence of some data appears to be best described by lines of negative slope, implying unphysical values of E_a. This is in qualitative agreement with studies of

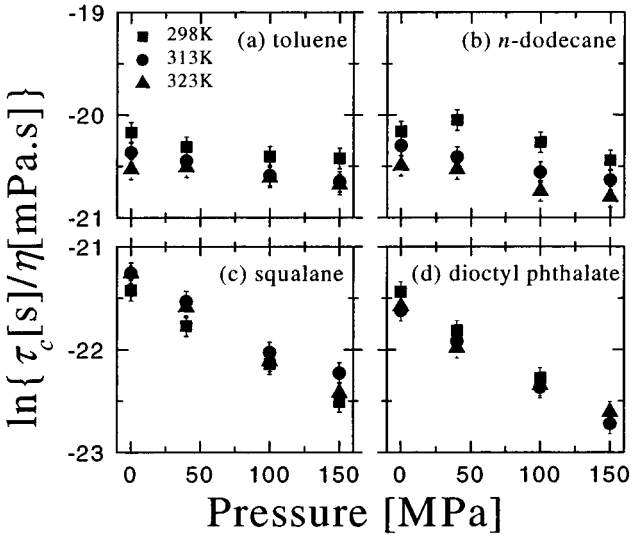

Figure 8. Plots of $\ln(\tau_c/\eta)$ as a function of P illustrating the failure of Kramers' theory in the high friction limit. The solvents are (a) toluene, (b) *n*-dodecane, (c) squalane, and (d) dioctyl phthalate at 298 K (squares), 313 K (circles), and 323 K (triangles).

the isomerization dynamics of various small molecules such as *trans*-stilbene,[47] 2VA,[48] 22PA,[49] and 1,4-diphenylbutadiene[50] which are also observed to scale as a fractional power of the solvent viscosity. Similar behavior is observed in Figure 8 for dynamics as a function of pressure at fixed temperatures.

A modified form of eq 7 that is able to describe the solvent scaling of these motions as a function of temperature at a fixed pressure (i.e., atmospheric pressure) has been proposed by Velsko et al.[51] as

$$\tau_c \sim \eta^{\alpha_T} \exp(E_a/RT) \tag{8}$$

When analyzing these motions as a function of pressure at a fixed temperature, eq 8 is recast as[26]

$$\tau_c \sim \eta^{\alpha_P} \exp(PV_a/RT) \tag{9}$$

where V_a is the intrinsic activation volume associated with the local dynamics. Differences between V_{obs} and V_a are attributed to contributions from the solvent's activation volume. The symbols α_T and α_P are used to avoid any implication at this stage that the viscosity scaling of the polymer motions as a function of temperature at a fixed pressure is similar to their scaling as a function of pressure at a fixed temperature.

To determine the value of α_T for the data in the present study, ln τ_c values for local dynamics within each solvent are plotted vs ln η at each temperature and pressure studied. Four of the possible 12 plots (i.e., three temperatures and four pressures) are shown in Figure 9. A value of α_T at each pressure is extracted as the average of the slopes of the three temperature plots at that pressure. The value of α_T was observed to be 0.65 $\pm$ 0.07 averaged over the four studied pressures. A value of E_a is determined at each pressure (i.e., each row of plots in Figure 9) by plotting the *y*-intercept of the ln τ_c vs ln η plots at temperatures 298, 313, and 323 K vs $1000/T$. These data are illustrated in Figure 10. The average value of E_a was found to be 12 $\pm$ 1 kJ mol^{-1} and independent of pressure within experimental error.

Values of α_P are extracted at each temperature as the average of the slopes of the four pressure plots in Figure 9 at that temperature. The average value of α_P was observed to be 0.65 $\pm$ 0.02 averaged over the three studied temperatures. A value of V_a is determined at each temperature (i.e., column in Figure 9) by plotting the *y*-intercept of the ln τ_c vs ln η plots at pressures of 0.1, 40, 100, and 150 MPa vs pressure. These data are illustrated in Figure 11. The average value of V_a was found to be 1.6 $\pm$ 0.6 cm^3 mol^{-1} and independent of temperature within experimental error.

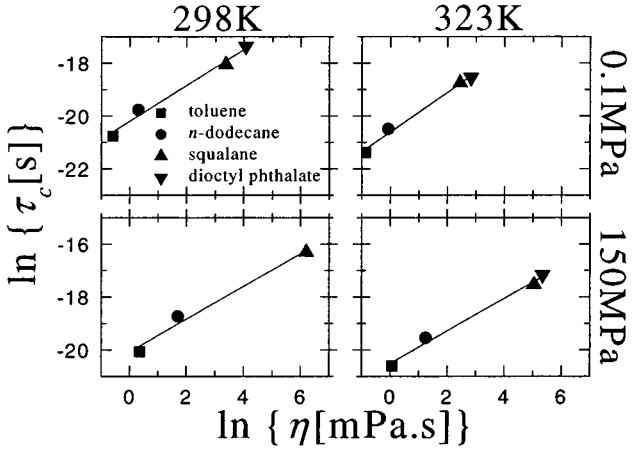

Figure 9. Four of the 12 possible plots (see text) of ln τ_c as a function of ln η. Each plot is generated from a value of τ_c for each of the solvents at a fixed temperature and pressure. The bottom left plot (lowest temperature and highest pressure studied) only contains data for toluene, *n*-dodecane, and squalane. The time scale for the local motions dioctyl phthalate at this temperature and pressure were too slow to allow a reliable value of τ_c to be determined.

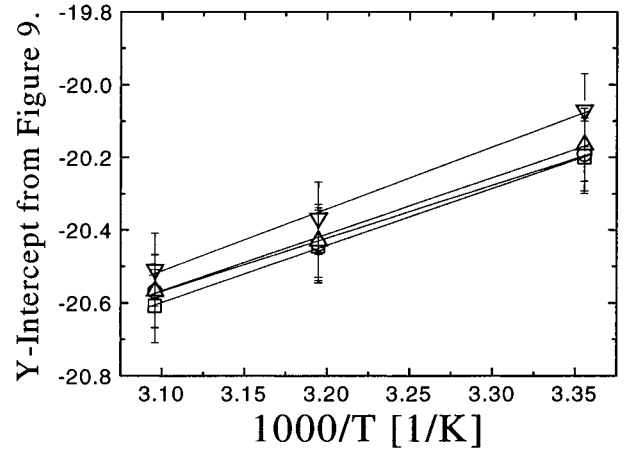

Figure 10. The *y*-intercept from ln τ_c vs ln η plots in Figure 9 plotted in Arrhenius format at four different pressures: 0.1 MPa (squares), 40 MPa (circles), 100 MPa (triangles), and 150 MPa (inverted triangles). The slope of each line is related to the activation energy E_a and yields a pressure-independent average value of 12 $\pm$ 1 kJ mol^{-1}.

IV. Summary

At the heart of this study is an investigation into the pressure dependence of the local segmental dynamics of *cis*-1,4-polyisoprene in dilute solution. This investigation was performed at three different temperatures revealing the dynamics obey

$$\tau_c(T,P) \sim \eta(T,P)^{0.65\pm0.05} \exp[(E_a + PV_a)/RT] \tag{10}$$

as illustrated in Figure 12, clearly indicating a violation

Table 4. Arrhenius Activation Energies, E_a, and Activation Volumes, V_a, Determined from the Slopes of Figures 10 and 11 as a Function of Pressure and Temperature, Respectively[a]

E_a [kJ mol^{-1}]					V_a [cm^3 mol^{-1}]			
0.1 MPa	40 MPa	100 MPa	150 MPa	av	298 K	313 K	323 K	av
13 (10[b])	12	13	12	12	2.0	1.2	1.6	1.6

[a] There is an error of ±10% associated with each value of E_a and of ±30% for each value of V_a. [b] Value of E_a at atmospheric pressure from Adolf et al.[19]

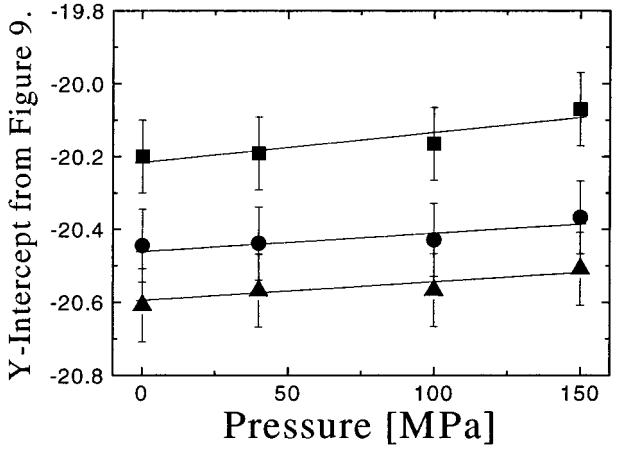

Figure 11. The *y*-intercept from ln τ_c vs ln η plots in Figure 9 plotted vs pressure at three temperatures: 298 K (squares), 313 K (circles), and 323 K (triangles). The slope of each line is related to the activation volume V_a and yields a temperature-independent average value of 1.6 ± 0.5 cm^3 mol^{-1}.

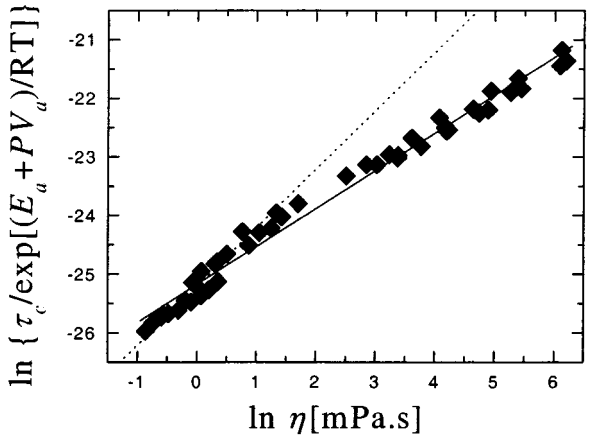

Figure 12. A master plot showing data for all four solvents at every temperature and pressure within this study. Values of E_a = 12 ± 1 kJ mol^{-1} and V_a = 1.6 ± 0.5 cm^3 mol^{-1} are utilized. The solid line is a fit to all the data and gives a value for α of 0.65 ± 0.05. The dotted line represents Kramer's theory in the limit of high friction (i.e., α = 1.00).

of Kramers' theory. The value of E_a was determined to be 12 ± 1 kJ mol^{-1}, and the value of V_a was found to be 1.6 ± 0.5 cm^3 mol^{-1} as reported in Table 4.

The value of the viscosity exponent in this study is slightly lower than that found by Adolf et al.[19] (α = 0.75 ± 0.06) of the local segmental dynamics of *cis*-1,4-polyisoprene performed only at atmospheric pressure over a similar temperature range and a slightly smaller viscosity range (0.44−300 mPa·s). This tendency for the exponent to decrease when considering systems at high pressure is in contrast to the work of Hara and co-workers on the isomerization of 2VA[25] and 22PA.[26] Measurements at 303 K up to 490 MPa revealed kinetics scale as $\eta^{0.2}$ for 2VA and $\eta^{0.40\pm0.02}$ for 22PA. Flom et al. and Kang et al. revealed $\eta^{\sim 0}$ for 2VA[49] and $\eta^{0.23}$ for 22PA[48] at atmospheric pressure. However, the work of Hara et al. did not employ the high viscosities or the wide viscosity range as found within this study.

The value of E_a (12 ± 1 kJ mol^{-1}) found in this study compares well with the value of 10 ± 1 kJ mol^{-1} also found by Adolf et al.[19] for this system using TROS. It is interesting to note that Glowinkowski et al.[13] determined a value of 13 ± 2 kJ mol^{-1} from ^{13}C NMR experiments on the same system. It is noted that V_a is significantly smaller than any value of V_{obs} (see Tables 3 and 4), which suggests that V_{obs} is dominated by the activation volume associated with the solvent viscosity in agreement with previous high-pressure investigations of small molecule isomerization.[25]

Further efforts into the effect of pressure on local polymer dynamics is currently focusing on solution and melt samples of *cis*-1,4-polybutadiene, *vinyl*-1,2-polybutadiene, polystyrene, and *cis*-1,4-polyisoprene. These data will appear in future publications.

Acknowledgment. This work was supported through funding from EPSRC GR/R17232 and the IRC in Polymer Science and Technology within the Department of Physics and Astronomy at the University of Leeds, UK. The authors are grateful to Dr. A. Kirpach for valuable discussions and for measurements which afforded some data within Figures 2 and 4.

References and Notes

(1) Adachi, K.; Kotaka, T. *Macromolecules* **1985**, *18*, 466.
(2) Adachi, K.; Okazaki, H.; Kotaka, T. *Macromolecules* **1985**, *18*, 1687.
(3) Adachi, K.; Kotaka, T. *Macromolecules* **1987**, *20*, 2018.
(4) Adachi, K.; Kotaka, T. *Macromolecules* **1988**, *21*, 157.
(5) Imanishi, Y.; Adachi, K.; Kotaka, T. *J. Chem. Phys.* **1988**, *89*, 7593.
(6) Adachi, K.; Imanishi, Y.; Shinkado, T.; Kotaka, T. *Macromolecules* **1989**, *22*, 2391.
(7) Adachi, K.; Imanishi, Y.; Kotaka, T. *J. Chem. Soc., Faraday Trans. 1* **1989**, *85*, 1065.
(8) Adachi, K.; Imanishi, Y.; Kotaka, T. *J. Chem. Soc., Faraday Trans. 1* **1989**, *85*, 1075.
(9) Adachi, K.; Imanishi, Y.; Kotaka, T. *J. Chem. Soc., Faraday Trans. 1* **1989**, *85*, 1083.
(10) Adachi, K. *Macromolecules* **1990**, *23*, 1816.
(11) Boese, D.; Kremer, F. *Macromolecules* **1990**, *23*, 829.
(12) Dejean de la Batie, R.; Lauprêtre, F.; Monnerie, L. *Macromolecules* **1989**, *22*, 122.
(13) Glowinkowski, S.; Gisser, D. J.; Ediger, M. D. *Macromolecules* **1990**, *23*, 3520.
(14) Lauprêtre, F.; Bokobza, L.; Monnerie, L. *Polymer* **1993**, *34*, 468.
(15) Hyde, P. D.; Waldow, D. A.; Ediger, M. D.; Kitano, T.; Ito, K. *Macromolecules* **1986**, *19*, 2533.
(16) Hyde, P. D.; Ediger, M. D.; Kitano, T.; Ito, K. *Macromolecules* **1989**, *22*, 2253.
(17) Vessier, V.; Viovy, J.-L.; Monnerie, L. *Polymer* **1989**, *30*, 1262.
(18) Waldow, D. A.; Johnson, B. S.; Hyde, P. H.; Ediger, M. D.; Kitano, T.; Ito, K. *Macromolecules* **1989**, *22*, 1345.
(19) Adolf, D. B.; Ediger, M. D.; Kitano, T.; Ito, K. *Macromolecules* **1992**, *25*, 867.
(20) Adams, S.; Adolf, D. B. *Macromolecules* **1998**, *31*, 5794.
(21) Adams, S.; Adolf, D. B. *Macromolecules* **1999**, *32*, 3136.
(22) Waldow, D. A.; Johnson, B. S.; Babiarz, C. L.; Ediger, M. D.; Kitano, T.; Ito, K. *Polym. Commun.* **1988**, *29*, 296.

(23) Kramers, H. A. *Physica* **1940**, *7*, 284.
(24) Waldow, D. A.; Ediger, M. D.; Yamaguchi, Y.; Matsushita, Y.; Noda, I. *Macromolecules* **1991**, *24*, 3147.
(25) Hara, K.; Kiyotani, H.; Kajimoto, O. *J. Chem. Phys.* **1995**, *103*, 5548.
(26) Hara, K.; Ito, N.; Kajimoto, O. *J. Phys. Chem. A* **1997**, *101*, 2240.
(27) Hara, K.; Akimoto, S.; Suzuki, H. *Chem. Phys. Lett.* **1990**, *175*, 493.
(28) Taniguchi, Y.; Senoo, M.; Hara, K. *High-Pressure Liquids and Solutions*; The Society of Materials Science: Japan, 1994.
(29) Viswanath, D. S.; Natarajan, G. *Data Book on the Viscosity of Liquids*; Hemisphere Publishing: New York, 1989.
(30) Barlow, A. J.; Lamb, J.; Matheson, A. J. *Proc. R. Soc. London A* **1966**, *292*, 322.
(31) Dr. N. F. Glen, National Engineering Laboratory, East Kilbride, Glasgow, G75 0QU.
(32) Tanaka, Y.; Hosokawa, H.; Kubota, H.; Makita, T. *Int. J. Thermophys.* **1991**, *12*, 245.
(33) Dymond, J. H.; Robertson, J.; Isdale, J. D. *Int. J. Thermophys.* **1981**, *2*, 133.
(34) Krahn, U. G.; Luft, G. *J. Chem. Eng. Data* **1994**, *39*, 670.
(35) O'Conner, D. V.; Philips, D. *Time-Correlated Single Photon Counting*; Academic Press: New York, 1984.
(36) Birch, D. J. S.; Imhof, R. E. *Topics in Fluorescence Spectroscopy*; Plenum: New York, 1991.
(37) Chong, P. L.-G.; Cossins, A. R. *Biochemistry* **1983**, *22*, 5544.
(38) Roy, P.; Roth, C. M.; Margolies, M. N.; Yarmush, M. L. *J. Biophys. Chem.* **1999**, *83*, 171.
(39) Mei, G.; Di Venere, A.; Campeggi, F. M.; Gilardi, G.; Rosato, N.; De Matties, F.; Finazzi-Agrò, A. *Eur. J. Biochem.* **1999**, *265*, 619.
(40) Castanho, M. A. R. B.; Prieto, M.; Jameson, D. M. *Biochim. Biophys. Acta* **1999**, *1419*, 1.
(41) Stapelfeldt, H.; Skibsted, L. H. *J. Dairy Res.* **1999**, *66*, 545.
(42) Sundaram, S.; Roth, C. M.; Yarmush, M. L. *Biotechnol. Prog.* **1998**, *14*, 773.
(43) Mateo, C. R.; Tauc, P.; Brochon, J.-C. *Biophys. J.* **1993**, *65*, 2248.
(44) Paladini, A. A.; Weber, G. *Rev. Sci. Instrum.* **1981**, *52*, 419.
(45) Hirayama, S.; Yasuda, H.; Okamoto, M.; Tanaka, F. *J. Phys. Chem.* **1991**, *95*, 2971.
(46) Adams, S. Ph.D. Thesis, The University of Leeds, Leeds, 1998.
(47) Rothenberger, G.; Negus, D. K.; Hochstrasser, R. M. *J. Chem. Phys.* **1983**, *79*, 5360.
(48) Brearley, A. M.; Flom, S. R.; Nagarajan, V.; Barbara, P. F. *J. Phys. Chem.* **1986**, *90*, 2092.
(49) Flom, S. R.; Nagarjan, V.; Barbara, P. F. *J. Phys. Chem.* **1986**, *90*, 2085.
(50) Velsko, S. P.; Fleming, G. R. *J. Chem. Phys.* **1982**, *76*, 3553.
(51) Velsko, S. P.; Waldeck, D. H.; Fleming, G. R. *J. Chem. Phys.* **1983**, *78*, 249.

MA011783R